Dalton Transactions

Accepted Manuscript

ROYAL SOCIETY OF CHEMISTRY

www.rsc.org/dalton

A pH-responsive Folate Conjugated Magnetic Nanoparticle for Targeted Chemo-thermal Therapy and MRI Diagnosis

Jagriti Gupta[a], Jeotikanta Mohapatra[b], Parag Bhargava[a] and D. Bahadur[a]*

[a]Department of Metallurgical Engineering and Materials Science
[b]Centre for Research in Nanotechnology and Science (CRNTS)
Indian Institute of Technology Bombay, Mumbai – 400076, India

*Corresponding author. Tel.: +91 22 2576 7632; Fax: +91 22 2572 3480.

E-mail address: dhirenb@iitb.ac.in

Abstract

Polyacrylic acid functionalized Fe_3O_4 nanoparticles (PAA-MNPs) of average size of 10 nm are prepared by a simple soft chemical approach. These PAA-MNPs are conjugated with folic acid through peptide bonding between the carboxylic group on the surface of PAA-MNPs and amine group of folic acid. The good colloidal stability of FA conjugated MNPs makes it a promising candidate for targeted drug delivery, hyperthermia and as MRI contrast agent with a transverse relaxivity R_2 value of 105 $mM^{-1}s^{-1}$. Folic acid conjugated magnetic nanoparticles (FA-MNPs) achieved ~ 95% loading efficiency of doxorubicin (DOX) which could be due to strong electrostatic interaction of highly negatively charged FA-MNPs and the positively charged DOX. The drug release study shows a pH-dependent behavior and is higher in acidic pH (4.3 and 5.6) as compared to the physiological pH (7.3). Flow cytometry and confocal microscopic image analysis reveal that around 75-80 % of HeLa cells undergo apoptosis due to DNA disintegration upon incubation with DOX-MNPs for 24 h. DOX-MNPs exhibit the synergistic effect due to the combination of DOX induced apoptosis and magnetic hyperthermia treatment (MHT) which enhance the cell death ~ 95.0 %. Thus, this system may serve as a potential pH sensitive nanocarrier for synergistic chemo-thermal therapy as well as a possible MRI contrast agent.

Keywords: *functionalization, magnetic nanoparticle, targeted drug delivery, chemo-thermal therapy and MRI contrast agent.*

1. Introduction

Iron oxide nanoparticles have been used as possible nanotheragnostic tool for tumor imaging (as MRI contrast agent), targeted drug delivery and thermotherapy of cancer (so-called hyperthermia) owing to its excellent bio-compatibility and unique superparamagnetic properties [1-4]. The MRI contrast agent and hyperthermia performance of magnetic nanoparticles (MNPs) have been improved by modifying the magnetic properties with control of size, shape and composition [4, 5]. Alternatively, these properties of MNPs are also modulated by surface functionalization, which minimizes aggregation, provides good aqueous stability, and bio-compatibility [6, 7]. The nonspecific distribution and adverse effects of anticancer drugs on normal tissues are the major challenges in the field of cancer chemotherapy. A variety of nanocarrier is developed to improve the treatment efficiency by transporting drugs specifically to tumors which in turn prevents undesired side effects [8, 9]. This unspecific delivery of drugs in chemotherapy causes harsh side effects in the cells. Targeted drug delivery systems enhance the selective drug delivery to the desired tissues, thereby minimizing drug accumulation at healthy tissues [6, 9]. MNPs when decorated with target molecules exhibit great potential for specific delivery and MR-imaging applications. Specific targeted ligands provide the selective binding of the drug carriers to the cell surface by triggering receptor-mediated endocytosis and enhancing cellular uptake of drug carrier [9, 10]. This could significantly enhance the efficiency for targeted thermo-chemotherapeutics. MNPs are able to generate heat under AC magnetic field which are useful for accumulating the drug to the desired site by using an external magnetic field [11]. Thus, the combination of hyperthermia (thermal therapy) with receptor mediated chemotherapy

has attracted remarkable interest due to their non-invasive methodology for the MR imaging and combination therapy.

Folic acid (FA) is a nontoxic, inexpensive, stable and low molecular weight nonimmunogenic receptor-specific ligand for anticancer drug because the surfaces of many human cancer cells are over-expressed by the folate-receptor [12-14]. On the other hand, the expression level of folate receptor is very low in normal cells [15]. Many folate-nanoparticles conjugated with polymeric nanoparticles, and carbon nanotubes, have already been reported [16, 17]. Alternatively, Stimuli-responsive drug release by magnetic nanoparticles have received much attention due to their various potential advantages like enhanced loading and release efficacy, reduced toxicity and side effects of therapeutic drugs [18]. Several nanocarriers have been reported with the purpose to respond to specific stimuli, such as pH, temperature, and enzymes [6, 9, 19]. Among these stimuli, pH response is the most universal as pH of different tissues and cellular organs change significantly. Furthermore, pH-responsive nanomaterials have the ability to entrap the drug molecules in the physiological or the extracellular environment, which helps to release the drug molecules in early endosomal and late endosomal/lysosomal region with lower pH (5.0–5.5). Functionalized magnetic nanoparticles (MNPs) are potential nanocarriers to efficiently deliver highly toxic chemotherapeutic drugs for cancer treatment at the site of interest. However, there are certain issues that should be addressed to improve the suitability of MNPs for clinical applications. Good colloidal stability and enhanced penetration capability of MNPs within physiological fluids in the tumor region ensure that their active targeting capability and stimuli-responsive performance are maintained in complex biological media. Particularly, from the view point of *in vivo* drug release behavior, many nanocarriers such

as peptides, nanohydrogels, mesoporous silica polymers, lipid, and dendritic molecules or core shell structures have been developed as a pH responsive delivery vehicle by exploiting slightly acidic tumor extracellular environment [20-28].

One of the greatest challenges in targeted drug delivery is to find out the optimal targeting agents that can selectively and successfully transport drug molecules to a particular type of cancerous tissue. Another desirable aspect of this strategy is the binding capability of targeting agents to the tumor cell surface in a suitable manner to trigger receptor endocytosis. The contribution of magnetic nanocarrier in cancer chemotherapy will certainly grow and provide more efficient tumor targeting strategies for cancer diagnosis and theranostic. This research work is focused on an active targeting agent, (folic acid) conjugated magnetic nanocarrier that offers both specific recognition and internalization of nanocarrier. We envisage that the folate conjugated magnetic nanocarriers are potentially useful for targeted drug delivery system with higher internalization and capability of delivering therapeutic agents (DOX) at targeted site particularly if these nanocarriers are stimulated by pH and AC magnetic field. The future prospects lies in minimizing undesirable side effects and improved therapeutic efficiency. Herein, we developed a simple biocompatible and an alternative pH-responsive targeted nanocarrier together with better targeting efficiency and quick release performance in mild acidic environment by a simple conjugation of polyacrylic acid functionalized MNPs with folic acid. The entrapment efficiency and drug release profile have been investigated. We further look into their colloidal stability, enhanced MRI contrast characteristics and heating capability under an external AC magnetic field. The results and the idea of using these FA-MNPs as a tool for combination therapy and diagnosis have been discussed in this paper.

2. Experimental section

Synthesis of iron oxide nanoparticles

Polyacrylic acid functionalized MNPs have been synthesized by one step co-precipitation method using $FeCl_3$ and $FeCl_2$. In this synthesis 4.4 g of $FeCl_3$ and 1.732g of $FeCl_2$ were added into 80 ml of water in a round bottom flask under nitrogen environment with constant stirring at 1000 rpm. The temperature was slowly increased to 70℃ and was maintained it for 30 min. After that 20 ml of (30 %) ammonia solution was added immediately in the above reaction mixture and kept at the same temperature for another 30 min. Then 4 ml of aqueous solution of polyacrylic acid (0.2g/ml) was added to the above reaction mixture. The reaction temperature was again increased up to 90℃ and hold at this temperature for 2 h with constant stirring. The obtained black coloured precipitates were cool down the reaction mixture to room temperature and rinsed thoroughly several times with water. Samples were separated after every wash with the help of a permanent magnet.

For the conjugation of folic acid, EDC/NHS coupling agent has been used. Polyacrylic acid functionalized MNPs were mixed with 75 mM of EDC and 15 mM of NHS solution and then the solution was shaken for 24 h at 2000 rpm to activate to carboxylic group. 2.5 mM folic acid in DMSO was added to the activated PAA-MNP solution and kept under constant stirring for 24 h in dark. After magnetic separation, the sample was rinsed several times with milli Q to remove the unattached folic acid and the sample (FA-MNPs) was dried at room temperature. FA-MNPs were further tagged with FITC to evaluate the uptake behavior of FA-MNPs. For the uptake analysis, FA-MNPs are dispersed in 200 µl FITC solution in 1 ml phosphate buffer solution having pH 8.5. Unbound dye was removed by repeated washing with phosphate

buffered saline (PBS, pH 7.4) followed by magnetic separation. The details of experimental procedures for drug delivery studies, and magnetic hyperthermia are described in supporting information.

3. Result and discussion

Fig. 1 (a) shows the XRD pattern of PAA-MNPs which indicates formation of single-phase inverse spinel structure. The obtained lattice constant of the PAA-MNPs (a = 8.377 Å) is similar to magnetite (ICDD card No. 88-0315, a = 8.375 Å). The crystallite size is estimated to be 10 nm using the Scherrer formula. Fig. 1 (b-d) shows the TEM micrograph of PAA-MNPs which reveal essentially spherical particles of size varying within 8-10 nm. HRTEM image (Fig. 1c) and the electron diffraction pattern (Fig. 1d) of PAA-MNPs also confirmed the crystalline nature of PAA-MNPs. From HRTEM, the average interfringe distance of PAA-MNPs is found to be ~0.30 nm which corresponds to (220) plane of inverse spinel Fe_3O_4.

Fig. 2 (a) shows the FTIR spectra of FA, PAA-MNPs, and FA-MNPs. Vibration band at 1710 cm^{-1} is recognized in PAA-MNPs for the C=O of O=C-OH group of PAA. Further the presence of vibrational band at 1610 cm^{-1} is assigned to O-H bending vibration of the O=C-OH group of PAA. Presence of these vibrational bands confirms the functionalization of the MNPs with PAA. Conjugation of PAA-MNPs with folic acid is also confirmed by the presence of bands at 1643 and 1697 cm^{-1} in FA-MNPs; indicating the amidation between carboxylate group of PAA-MNPs with the amine group of folic acid. Further the conjugation of folic acid with PAA-MNPs is also confirmed by the presence of band at 1604 cm^{-1} corresponds to the stretching vibration of aromatic ring. Fig. 2 (b) shows the TGA analysis of PAA-MNPs, FA-MNPs and DOX-MNPs. Weight loss in PAA-MNPs at low temperature ($\leq 150^{\circ}C$) can be attributed due to

the removal of physically attached water molecule on the surface of MNPs. Weight loss of about 10 % in PAA-MNPs at the higher temperature of about 300 $^{\circ}$C can be attributed due to the removal of chemically bonded PAA molecule on the surface of MNPs. In FA-MNPs, weight loss increases by ~ 37 %, attributed to the presence of more contents of organic moieties on the surface of the MNPs. Further increase in the weight loss ~ 50.7 % in the DOX-MNPs is due to the loss of DOX molecule electrostatically attached on the surface of FA-MNPs. Functionalization of PAA-MNPs with the folic acid is also confirmed by the appearance of the characteristic UV-visible absorption peaks of FA at 280 and 370 nm (See ESI Fig.S1).

Fig. 3 (a) shows the room temperature magnetization (M *vs.* H) plots of PAA-MNPs and FA-MNPs. The magnetization of PAA-MNPs and FA-MNPs were found to be 56 and 44 emu/g at 20 kOe, respectively. The magnetization curve (inset of Fig. 3 a-i) shows the typical superparamagnetic properties with zero coercivity and remanence. Fig. 3 (b-ii) shows the zero field cooled (ZFC) and field cooled (FC) magnetization plot of PAA-MNPs and FA-MNPs measured at a field of 100 Oe. The blocking temperature for both PAA-MNPs and FA-MNPs are found to be 180 K. Since the prepared MNPs are monodisperse ($\sigma < 15$ %), the broadening of the ZFC peak could be attributed to the dipolar interaction between single domain particles of very high magnetic moment (10^2-10^3 μ_B/particles) [4]. Furthermore, the decrease in the magnetization from PAA-MNPs to FA-MNPs (from 56 to 44 emu/g) is due to presence of additional organic moieties (folic acid) on the surface of PAA-MNPs. This again confirms the conjugation of FA molecules with PAA-MNPs, as suggested by the FITR spectra, TGA analysis and UV-visible spectra. Fig. 3 (b) shows the Zeta potential of PAA-MNPs and FA-MNPs at different pH. The PAA molecule absorbed on the surface of magnetic nanoparticles makes the

surface of Fe_3O_4 highly negative. The observed negative Zeta potential at high pH is probably due to the presence of negatively charged carboxylate ions on the surface of the MNPs. Further functionalization of PAA-MNPs with the FA, makes the zeta potential more negative which indicates conjugation of amine group of FA with the acid group of PAA-MNPs.

The T_2-weighted MR images of FA-MNPs recorded at 3 Tesla show significant signal attenuation with increasing concentration of iron from 0.004 to 0.05 mM as shown in Fig. 4 (a). Even at a very low Fe concentration, the FA-MNPs show a strong T_2 signal intensity and increases with the increase in Fe concentration. As expected, the relaxation rate varies linearly with the Fe concentration and the calculated R_2 value of FA-MNPs is 105 mM^{-1} s^{-1} (Fig. 4b). The observed R_2 relaxivity value is higher by 20 mM^{-1} s^{-1} than that of the commercial contrast agent (85 mM^{-1} s^{-1}) [29]. It was reported that the surface modification of Fe_3O_4 nanoparticles can significantly improve the transverse relaxivity which could be advantageous for its use as T_2 contrast agent in MRI. For example, Basly *et al.* synthesized dendrimer functionalized Fe_3O_4 nanoparticles by conjugating PEGylated dendrons onto the surface of Fe_3O_4 nanoparticles through a phosphonate anchor and observed a high R_2 relaxivity of 349 mM^{-1} s^{-1} at 1.5 T [30]. Hence, the high relaxivity of FA-MNPs, observed in the present case, could be attributed to the good magnetization of Fe_3O_4 core and the folic acid conjugation with PAA, which brings in good colloidal stability. Thus the high R_2 value and excellent colloidal stability make the FA-MNPs promising candidates for high-efficiency T_2–weighted contrast agent in MR imaging application.

Cellular uptake of FA-MNPs was investigated using confocal laser scanning microscopy (CLSM) and ICP-AES analysis. The cellular uptake behaviour of FA-MNPs has been performed in two different cell lines in which cancerous cells (HeLa cells) are over expressed by folate

receptor used as positive control and Normal cells (L929 cells) is only minimally distributed by folate receptor used as negative control [2]. Moreover, for HeLa and L929 cells, the uptake of materials depends on the surface receptor present on the cells surface. L929 cells are used as folate receptor negative for the control experiment. Fig. 5 (a) shows the CLSM image of HeLa cells after incubation for 4 h with the FITC labeled FA-MNPs. A significant uptake of FA-MNPs was seen from the green fluorescence image arising from FITC emissions, suggesting that the FITC labeled nanoparticles were internalized in the cells. The cellular uptake of DOX-MNPs was also quantified by measuring the iron content per cell using ICP-AES analysis. Fig. 5 (b) shows the uptake behavior of FA-MNPs in terms of Fe Concentration in pg/cells. From the ICP-AES analysis, it has been observed that the cellular uptake or internalization of FA-MNPs in HeLa cells is higher as compared to L929 due to the presence of folate receptor cells that suggest the cancer specificity nature of folate conjugated magnetic nanoparticles and confirm the internalization of particles through the receptor mediated endocytosis.

Fluorescence spectroscopy was used to evaluate the loading efficiency and interaction of drug molecules with FA-MNPs which has been shown in Fig. S2.The fluorescence intensity of DOX starts to decrease in the presence of FA-MNPs, confirming the interaction between DOX and FA-MNPs, whereas no self-quenching was observed in pure DOX due to p–p stacking between DOX molecules. The loading efficiency (DOX with FA-MNP) calculated from fluorescence spectra are shown in Fig. S3. The loading capacity is strongly dependent on particles to DOX ratio in solution and ~ 95 (w/w) % loading efficiency is achieved in FA-MNPs. This higher loading efficiency is due to strong electrostatic interaction between the positively

charged DOX molecules and the negatively charged carboxylic moieties present on the surface of FA-MNPs [7].

pH responsive release of DOX from DOX-MNPs has been investigated in PBS solution at different pH (pH 4.3, 5.6 and 7.4 at 37 ℃) as shown in Fig. 6. Our drug release results show that very little amount of DOX is released at pH 7.4 (~ 3 % in 4h and 10 % DOX in 60 h). In contrast to this, release of DOX is increased under acidic pH (5.6) (~ 23% at 4h and 86% at 60h) and further at pH 4.5, the amount of DOX released is a significantly higher in the same time period (~ 39 % in 4h and 98 % in 60h). It has been observed that DOX-MNPs shows good release performance under acidic pH and very less amount of DOX is released under physiological pH as compared to the previously reported work [31-34]. Therefore, this material is very effective for drug release at a particular site of interest that helps to reduce the side effect of the chemotherapeutic drugs. From this, it has been established that FA-MNPs efficiently worked to prevent undesired release of drug molecules in the physiological environment (pH 7.4) and achieved a rapid release in endosomal environment (pH 4.3–5.6). Interestingly, it has been found that the release rate of DOX is higher at lower pH. After internalization into the acidic endosomal environment, the DOX-MNPs undergo pH-responsive release and then penetrate into the cytosol. Probably, the drug release in the acidic environment of endosomes is due to the dwindling of the electrostatic interactions between the drug molecules and the partly neutralized carboxylic groups on the surface of FA-MNPs. Potentially these nanocarriers not only minimize adverse effects of drug but also increase specific accumulation in targeted tissue by the enhanced permeation and retention (EPR) effect. This is advantageous for cancer therapy because it specifically stimulates the release of DOX to the target site at low pH in tumors. At physiological

pH 7.3, a modest release of ~10% is observed due to stability of electrostatically bound drug molecules (DOX-MNPs). However, essentially a complete release at pH 4.3 and pH 5.6 is observed. Furthermore, this pH triggered release of DOX from the DOX-MNPs may help to reduce the side effects of drug to the normal cells and enhance the tumor selectivity towards cancer cells.

Cytotoxicity behavior of FA-MNPs, DOX and DOX-MNPs has been investigated using SRB assay. Our biocompatibility results showed that more than 95% of cells are viable even after 24 h incubation with 2 mg/ml of FA-MNPs (See Fig. S4a, EIS). HeLa cells do not show any change in cellular morphology as depicted from the optical microscopic images. Thus, the cell viability is not much affected in the presence of FA-MNPs, suggesting that FA-MNPs are biocompatible and do not have any toxic effect on HeLa cells (See Fig. S5b, EIS). On the other hand, DOX-MNPs show significant toxicity to cell proliferation. Fig. S4 (b) shows the cytotoxic effect of DOX and DOX-MNPs on HeLa cells. The optical microscopic images of HeLa cells also suggest that the control cells grow without any loss in the cell membrane integrity. In contrast to this, HeLa cells on treatment with DOX-MNPs show a significant change in the morphology. The optical image shows that the cell's morphology becomes spherical on treatment with DOX-MNPs. This type of change in the morphology suggests that the cells undergo the apoptosis process (See Fig.5e, EIS).

To enhance the chemotherapic effect of DOX-MNPs, magnetic hyperthermia has been employed to investigate the synergistic effect. Fig. 7 (a) shows the temperature *vs.* time plot of FA-MNPs in PBS and DMEM under AC magnetic field (ACMF). The results show a gradual increase in temperature with respect to time. The thermal therapy depends on the heating

efficiency of MNPs, which is expressed in terms of the specific absorption rate (SAR). The SAR of FA-MNPs in PBS (2 mg/ml) is determined in a field strength of 338 Oe and is found to be 39.4 W/g. The collective effects of hyperthermia and chemotherapy were performed by using HeLa cells as shown in Fig. 7 (b). It has been found that the control cells with and without ACMF does not show much decrease in cell viability. Conversely, cells loaded with FA-MNPs, DOX and DOX-MNPs showed decrease in cell viability significantly as expected. In the presence of ACMF, DOX-MNPs and FA-MNPs showed ~ 90.5% and 35% decrease in cell viability, respectively. It has been found that DOX-MNPs in combination with ACMF show much higher cytotoxicity (i.e. 90.5% decreases in cell proliferation) than individual treatments of FA-MNPs with ACMF and DOX-MNPs. The enhanced drug release in the presence of AC magnetic field is known in the literature [35]. This synergetic effect of hyperthermia under ACMF helps to break bond and thereby enhance the drug release. Magnetic hyperthermia not only enhances the chemotherapeutic effect but also disrupts the cytoplasm regions due to accumulation of significant amount of drugs in the nucleus. Heating effect may also damage many cellular components like cell membrane, cytoskeleton and enzymes that are required for DNA synthesis [6]. Thus, heat and drug accumulation helps to enhance maximum cell death simultaneously and synergistically. From the optical images, rounded cells with disrupted membrane under ACMF confirm that the cells undergo the apoptosis process.

Further to confirm the apoptosis due to the synergistic effect of thermo chemotherapy, flow cytometric analysis and confocal microscopy have been performed. Fig. 8 shows the FACS analysis of HeLa cells post treatment with DOX, FA-MNPs and DOX-MNPs in presence and absence of ACMF. FA-MNPs show very little influence on the apoptosis of HeLa cells.

Apoptotic cells under treatment with FA-MNPs, DOX-MNPs with or without ACMF were quantitatively analyzed using FITC-Annexin and PI staining. From the FACS analysis, it has been found that no apoptosis occurs after 24 h exposure in the HeLa control cells. However, when the cells were treated with DOX, ~ 75.7 % apoptotic cells were observed after 24 h exposure. Further, HeLa cells on treatment with DOX-MNPs, about 61.3 % cells undergo apoptosis whereas if combined with application of ACMF about 95 % apoptotic cells are found. The apoptotic cells are also confirmed by confocal microscopy by using nucleus staining with Ethidium bromide. Fig. 9 (a) shows cells without any treatment. It shows that cells are viable with intact nuclear membranes. Fig. 9 (b-c) shows the confocal images of HeLa cells treated with DOX for 3 and 48h whereas Fig. 9 (d-f) gives the confocal images of HeLa cells treated with DOX-MNPs for 3, 24 and 48h. These confocal images demonstrate damaged cell membrane with complete DNA fragmentation and a reduction in size of the nucleus of HeLa cells on treatment with DOX and DOX-MNPs as the time of treatment increases from 3 to 48 h. These prominent morphological features are used as credentials of apoptosis in cancer cells. Similar apoptotic features such as change in morphology and lost adhesion from the cell culture plate are also seen in the optical images. The observed levels of cellular shrinkage or rounding are the clear indications of apoptotic cells (See Fig. S5 d-f, ESI). DNA fragmentation in HeLa cells using DOX loaded mesoporous magnetic nanoassemblies (MMNs) and DOX loaded dextran coated MNPs has been reported by Kumar *et al.* and Li *et al.* [3, 36]. Our cytotoxicity study shows that DOX-MNPs are less toxic than the free DOX. The free DOX diffuses into the cytoplasm and enters through P-glycoprotein efflux pump whereas DOX-MNPs are internalized *via* receptor mediated endocytosis and localized in cytoplasm and then diffused into nucleus [37-

39]. Drug efflux is a major stumbling block for effective chemotherapy. DOX-MNPs not only reduce the toxic effects of free DOX but also enhance the therapeutic efficacy and increase the DOX retention time inside cancer cells. Thus DOX-MNPs can be potentially used for combined effect of magnetic hyperthermia and chemotherapy.

4. Conclusions

We have developed folate conjugated magnetic nanoparticles (FA-MNPs) of average size of ~ 10 nm and studied its performance for pH-triggered and targeted drug release, thermal therapy and in MR imaging. Folate conjugated magnetic nanoparticles show high loading efficiency due to the highly negatively charged surface. The drug release results showed that DOX is quickly released in an acidic environment (pH 4.3-5.6) as compared to a physiological environment (pH 7.4), which causes significant cytotoxicity to cancer cells. This formulation enhances drug accumulation at intercellular compartments of tumor cells with low drug concentration in the normal cells. Thus, the folate conjugated magnetic nanoparticles with pH responsive behavior may be useful as a good carrier combining the chemotherapy and hyperthermia. This synergistic effect of chemo thermal-therapy is significantly enhanced as compared to the individual chemo and thermal therapy.

Acknowledgement

Jagriti Gupta acknowledges CSIR, India for the award of Senior Research Fellowship (SRF).The financial support by Nanomission of DST, and nanotechnology division of DEITY, Government of India are gratefully acknowledged.

References:

[1] L. Zhu, D. Wang, X. Wei, X. Zhu, J. Li, C. Tu, Y. Su, J. Wu, B. Zhu and D. Yan, *J. Controlled Release*, 2013, **169**, 228-238.

[2] D. Bhattacharya, M. Das, D. Mishra, I. Banerjee, S. K. Sahu, T. K. Maiti and P. Pramanik, *Nanoscale*, 2011, **3**, 1653-1662.

[3] S. Kumar, A. Daverey, N. K. Sahu and D. Bahadur, *J. Mater. Chem. B*, 2013, **1**, 3652-3660.

[4] J. Mohapatra, S. Nigam, J. Gupta, A. Mitra, M. Aslam and D. Bahadur, *RSC Adv.*, 2015, **5**, 14311-14321.

[5] J. Mohapatra, A. Mitra, H. Tyagi, D. Bahadur and M. Aslam, *Nanoscale*, 2015, **7**, 9174-9184.

[6] L. Pradhan, R. Srivastava and D. Bahadur, *Acta Biomater.*, 2014, **10**, 2976-2987.

[7] K. C. Barick, S. Singh, N. V. Jadhav, D. Bahadur, B. N. Pandey and P. A. Hassan, *Adv. Funct. Mater*, 2012, **22**, 4975-4984.

[8] Y. Zhu, Y. Fang and S. Kaskel, *J. Phys. Chem. C*, 2010, **114**, 16382-16388.

[9] J. Gupta, P. Bhargava and D. Bahadur, *J. Appl. Phys.*, 2014, **115**, 17B516-517B516-513.

[10] J. D. Byrne, T. Betancourt and L. Brannon-Peppas, *Adv. Drug Delivery Rev.*, 2008, **60**, 1615-1626.

[11] J. Dobson, *Drug Dev. Res*, 2006, **67**, 55-60.

[12] J. Sudimack and R. J. Lee, *Adv. Drug Deliv. Rev.*, 2000, **41**, 147-162.

[13] J. J. Turek, C. P. Leamon and P. S. Low, *J. Cell Sci.*, 1993, **106**, 423-430.

[14] A. C. Antony, *Blood*, 1992, **79**, 2807-2820.

[15] H. S. Yoo and T. G. Park, *J.Controlled Release*, 2004, **100**, 247-256.

[16] H. Song, C. Su, W. Cui, B. Zhu, L. Liu, Z. Chen and L. Zhao, *Biomed Res Int*, 2013, **2013**, 6.

[17] L. Niu, L. Meng and Q. Lu, *Macromol Biosci,*, 2013, **13**, 735-744.

[18] R. D. J. Ajeet Kaushik, Vidya Sagar and Madhavan Nair, *Expert Opin. Drug Deliv.*, 2014, **11**, 1635-1646.

[19] M. K. Jaiswal, A. Pradhan, R. Banerjee and D. Bahadur, *J. Nanosci. Nanotechnol.*, 2014, **14**, 4082-4089.

[20] X. Chen, L. Chen, X. Yao, Z. Zhang, C. He, J. Zhang and X. Chen, *Chem. Commun.*, 2014, **50**, 3789-3791.

[21] M. Colilla, B. Gonzalez and M. Vallet-Regi, *Biomater. Sci.*, 2013, **1**, 114-134.

[22] Q. He, Y. Gao, L. Zhang, Z. Zhang, F. Gao, X. Ji, Y. Li and J. Shi, *Biomaterials*, 2011, **32**, 7711-7720.

[23] J. H. Maeng, D. H. Lee, K. H. Jung, Y. H. Bae, I. S. Park, S. Jeong, Y. S. Jeon, C. K. Shim, W. Kim, J. Kim, J. Lee, Y. M. Lee, J. H. Kim, W. H. Kim and S. S. Hong, *Biomaterials*, 2010, **31**, 4995-5006.

[24] Q. Liu, H. Zhu, J. Qin, H. Dong and J. Du, *Biomacromolecules*, 2014, **15**, 1586-1592.

[25] D. Pan, W. she, C. Guo, K. Luo, Q. Yi and Z. Gu, *Biomaterials*, 2014, **35**, 10080-10092.

[26] K. Chatterjee, S. Sarkar, K. Jagajjanani Rao and S. Paria, *Adv. Colloid Interface Sci.*, 2014, **209**, 8-39.

[27] L. Momtazi, S. Bagherifam, G. Singh, A. Hofgaard, M. Hakkarainen, W. R. Glomm, N. Roos, G. M. Mælandsmo, G. Griffiths and B. Nyström, *J. Colloid Interface Sci.*, 2014, **433**, 76-85.

[28] N. K. Sahu, J. Gupta and D. Bahadur, *Dalton Trans.*, 2015, **44**, 9103-9113.

[29] K. C. Barick, M. Aslam, Y.-P. Lin, D. Bahadur, P. V. Prasad and V. P. Dravid, *J. Mater. Chem.*, 2009, **19**, 7023-7029.

[30] B. Basly, D. Felder-Flesch, P. Perriat, C. Billotey, J. Taleb, G. Pourroy and S. Begin-Colin, *Chem. Commun.*, 2010, **46**, 985-987.

[31] Y. J. Lu, K. C. Wei, C. C. Ma, S. Y. Yang and J. P. Chen, *Colloids and surfaces. B, Biointerfaces*, 2012, **89**, 1-9.

[32] F. M. Kievit, F. Y. Wang, C. Fang, H. Mok, K. Wang, J. R. Silber, R. G. Ellenbogen and M. Zhang, *J. Controlled Release*, 2011, **152**, 76-83.

[33] H. Tang, J. Guo, Y. Sun, B. Chang, Q. Ren and W. Yang, *Int. J. Pharm.*, 2011, **421**, 388-396.

[34] C. Fang, F. M. Kievit, O. Veiseh, Z. R. Stephen, T. Wang, D. Lee, R. G. Ellenbogen and M. Zhang, *J. Control Release*, 2012, **162**, 233-241.

[35] S. Chandra, S. Mehta, S. Nigam and D. Bahadur, *New J. Chem.*, 2010, **34**, 648-655.

[36] Y.-L. Li, L. Zhu, Z. Liu, R. Cheng, F. Meng, J.-H. Cui, S.-J. Ji and Z. Zhong, *Angew. Chem. Int. Ed.*, 2009, **48**, 9914-9918.

[37] Y. Tian, L. Bromberg, S. N. Lin, T. A. Hatton and K. C. Tam, *J. Controlled Release* 2007, **121**, 137-145.

[38] Y. Gao, Y. Chen, X. Ji, X. He, Q. Yin, Z. Zhang, J. Shi and Y. Li, *ACS Nano*, 2011, **5**, 9788-9798.

[39] S. R. Yang, H. J. Lee and J.-D. Kim, *J. Controlled Release*, 2006, **114**, 60-68.

Figure Caption:

Fig.1. (a) XRD pattern, (b) TEM micrograph, (c) HR-image, and (d) SAED pattern of PAA-MNPs.

Fig.2. (a) FTIR spectra of FA, PAA-MNPs, and FA-MNPs, and (b) TGA spectra of FA-MNPs, PAA-MNPs, and DOX-MNPs.

Fig.3. (a) Field dependent magnetization (*M vs. H*)plot, (a-i) inset shows expanded M *vs.* H plot at the low-field region and (a-ii) inset shows Zero field cooled-field cooled (ZFC-FC) plot of PAA-MNPs and FA-MNPs at 300 K and (b) Zeta potential of PAA-MNPs and FA-MNPs.

Fig.4. MR contrast effect of FA-MNPs (a) T_2-weighted MR images of at various concentrations of iron under an applied magnetic field of 3 T, TR = 3500 ms and TE = 45 ms. (b) Plots of $1/T_2$ values at various concentrations of iron.

Fig.5. Drug release profile of DOX-MNPs in different pH conditions (pH-4.3.5.6 and 7.3) at 37℃.

Fig.6. (a) Cellular uptake behaviour of FITC labeled FA-MNPs by HeLa cells after incubation for 4 h, and (b) Quantification of cellular uptake of FA-MNPs in HeLa and L929 by measuring the iron content per cell using ICP-AES analysis.

Fig.7. (a) Temperature vs. time plots of aqueous suspension of FA-MNPs (2 mg/ml of FA-MNPs) at a field of 338 Oe in PBS and DMEM media and (b) Cell viabilities of HeLa cells after treatment with DOX, FA-MNPs and DOX-MNPs with and without application of ACMF.

Fig.8. FACS analysis representing apoptosis based on Annexin V-FITC and PI staining assay of (a) Control HeLa cells (b) treated with DOX, (c) DOX-MNPs, (d) FA-MNPs, (e) FA-MNPs with ACMFand (f) DOX-MNPs with ACMF.

Fig.9. Confocal laser scanning microscopy (CLSM) images show the apoptosis (DNA fragmentation) in (a) Control HeLa cells showing rounded, intact nucleus, (b-c) with DOX (7μg/ml) at indicated time intervals of 3 and 48 h, (d-e) with DOX-MNPs (100μg/ml) at indicated time intervals of 3, 24 and 48 h. The green fluorescence shows the presence of DOX in DOX-MNPs, red fluorescence shows ethidium bromide (EtBr) stained nuclei. The scale bar is 50 μm.

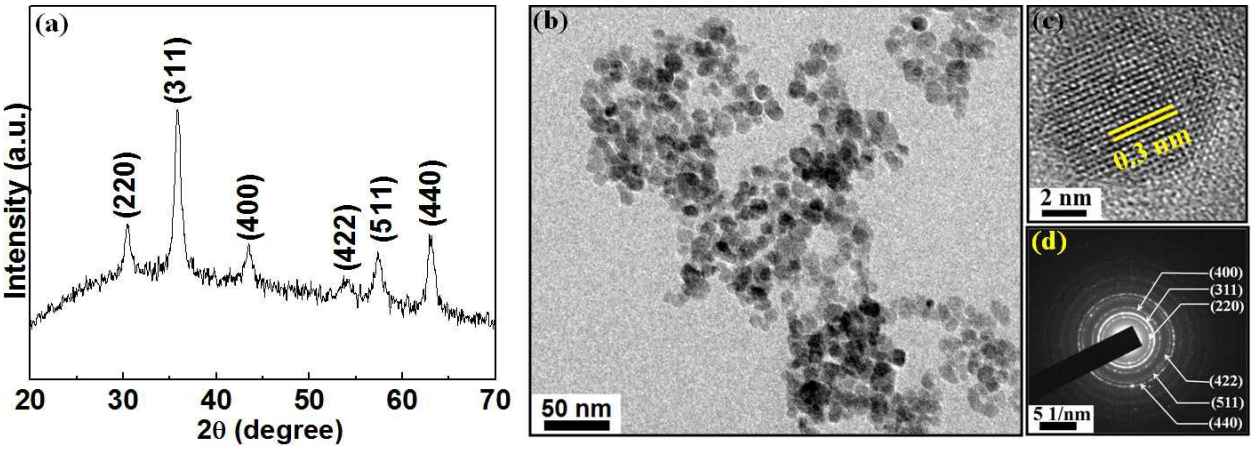

Fig.1. (a) XRD pattern of PAA-MNPs, (b) TEM micrograph of PAA-MNPs, (c) HR-image of PAA-MNPs, and (d) SAED pattern of PAA-MNPs.

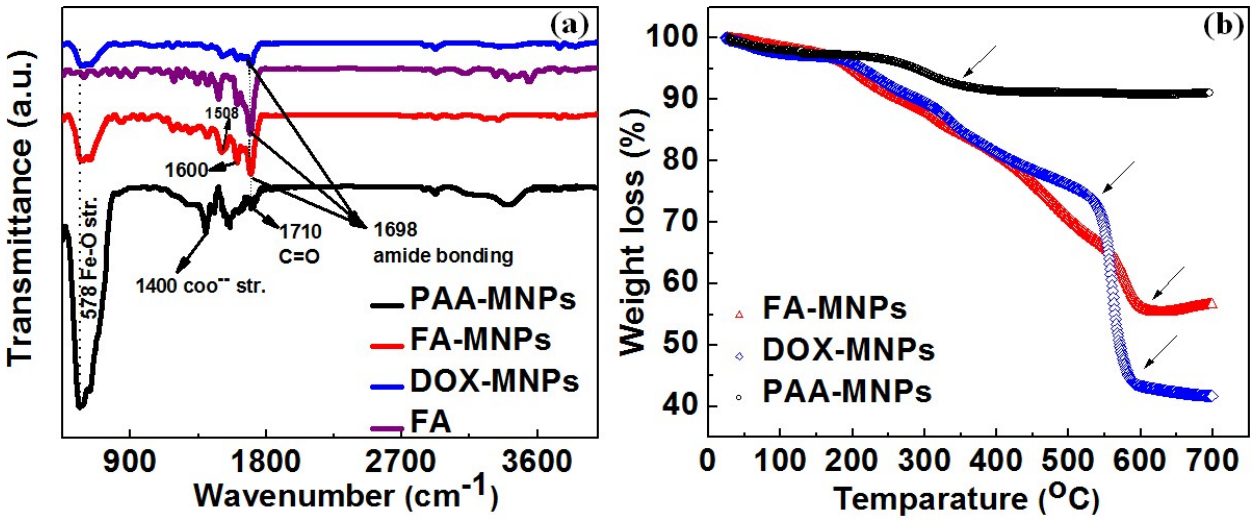

Fig.2. (a) FTIR spectra of FA, PAA-MNPs, FA-MNPs, and (b) TGA plot of FA-MNPs, PAA-MNPs, and DOX-MNPs.

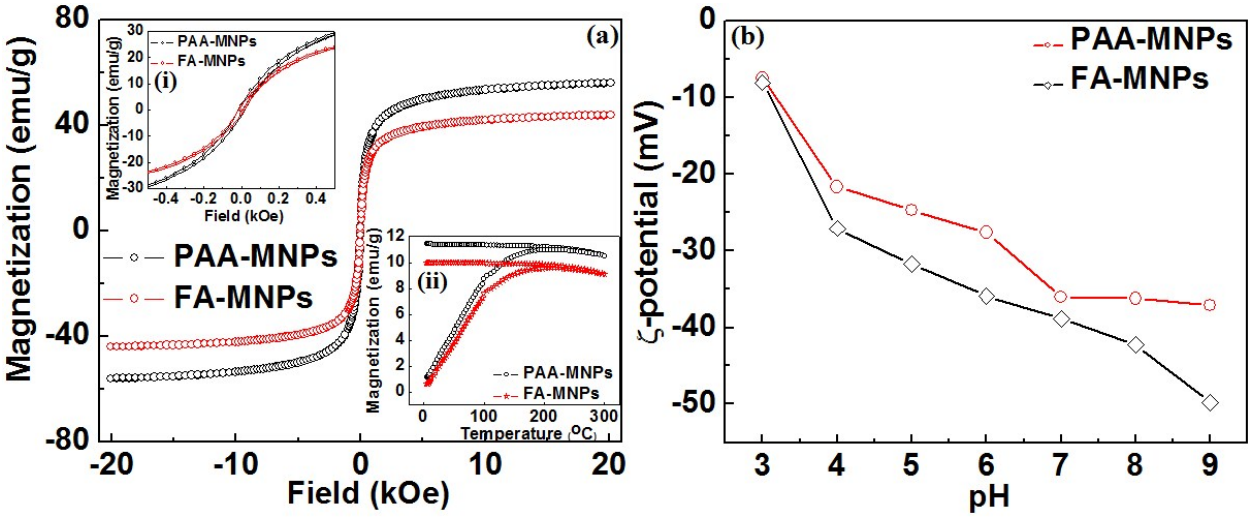

Fig.3. (a) Field dependent magnetization (M *vs.* H) plot at 300 K, (a-i) inset shows expanded M *vs.* H plot in the low-field region showing coercivity and (a-ii) inset shows Zero field cooled-field cooled (ZFC-FC) plot of PAA-MNPs and FA-MNPs and (b) Zeta potential of PAA-MNPs and FA-MNPs as a function of pH.

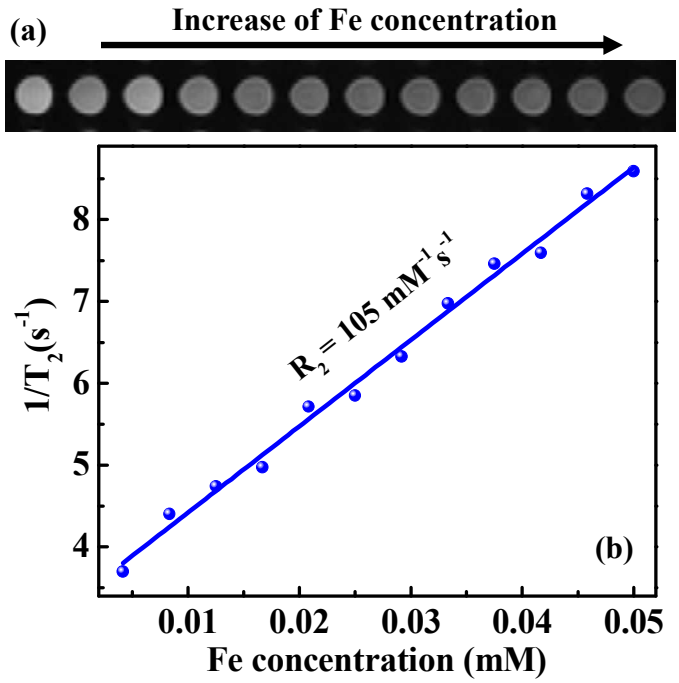

Fig.4. MR contrast effect of Fe_3O_4 FA-MNPs: (a) T_2-weighted MR images of at various concentrations of iron under an applied magnetic field of 3 T, TR = 3500 ms and TE = 45 ms. (b) Plots of $1/T_2$ values at various concentrations of iron.

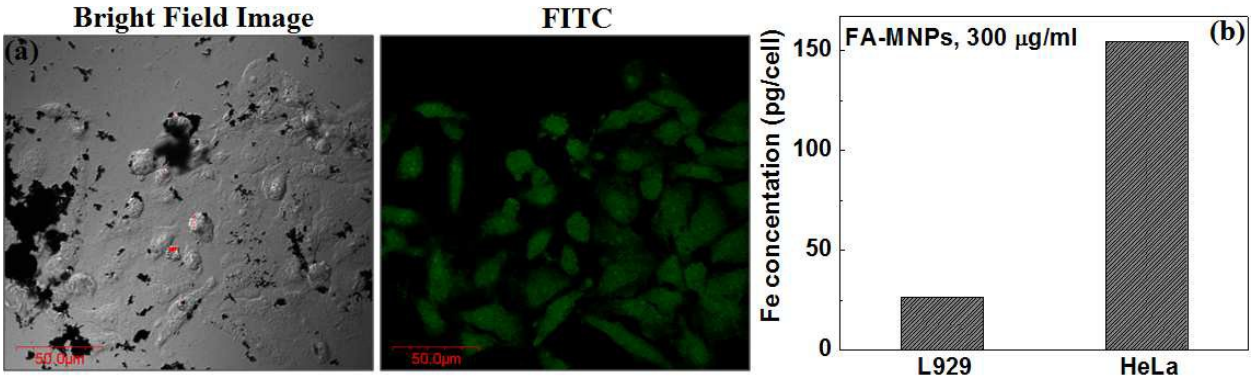

Fig.5. (a) Cellular uptake behavior of FITC labelled FA-MNPs in HeLa cells after 4 h incubation, and (b) Quantification of cellular uptake of FA-MNPs in HeLa and L929 by measuring the iron content per cell using ICP-AES analysis.

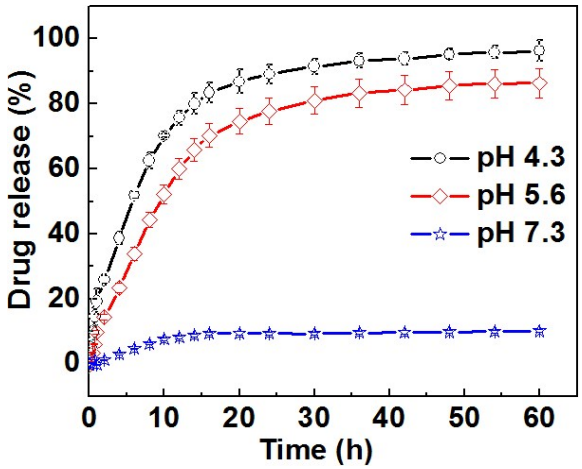

Fig.6. Drug release profile of DOX-MNPs in different pH conditions (pH-4.3,5.6 and 7.3) at 37 ℃.

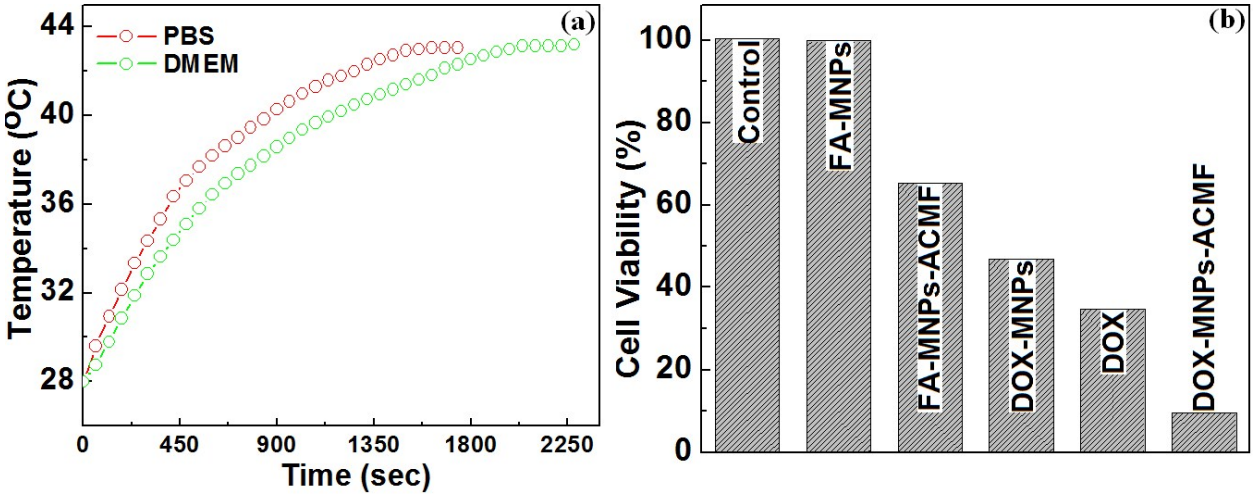

Fig.7. (a) Temperature *vs.* time plots of FA-MNPs (2 mg/ml of FA-MNPs) at a field of 338 Oe in PBS and DMEM media and (b) Cell viabilities of HeLa cells after treatment with DOX, FA-MNPs and DOX-MNPs with and without application of ACMF.

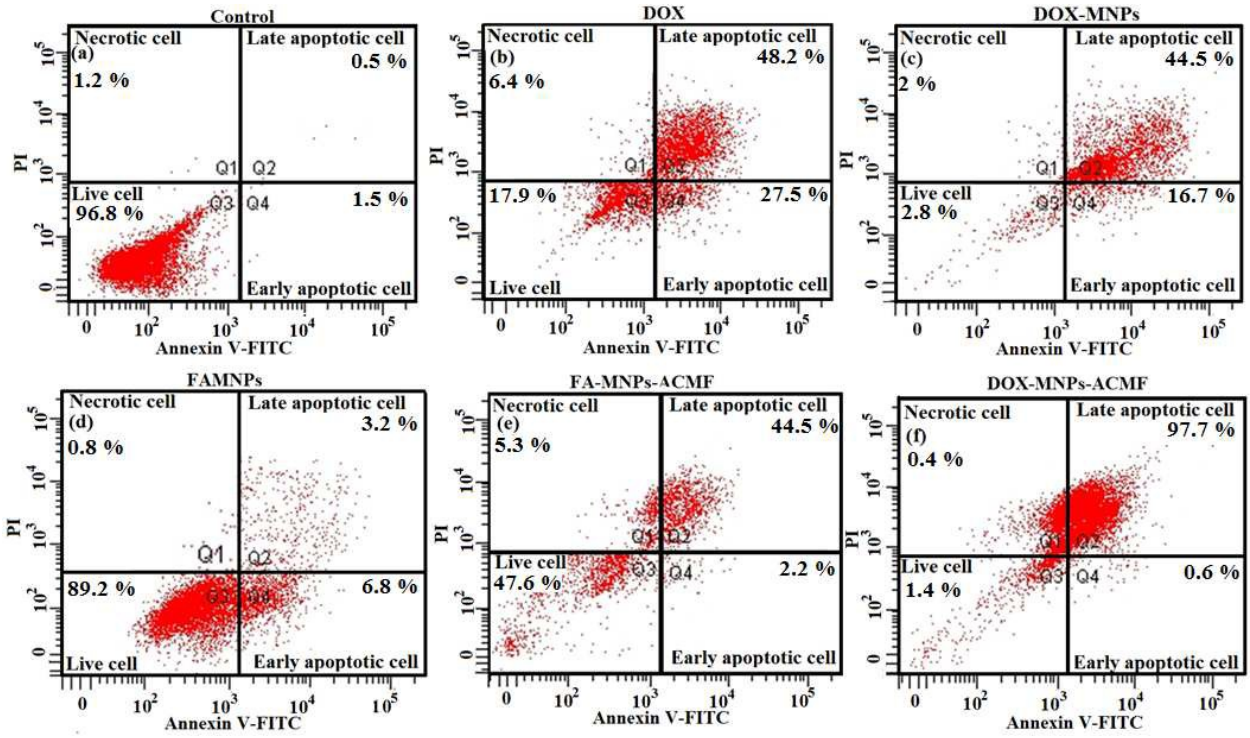

Fig.8. FACS analysis representing apoptosis based on Annexin V-FITC and PI staining assay of (a) Control HeLa cells (b) treated with DOX, (c) DOX-MNPs, (d) FA-MNPs, (e) FA-MNPs with ACMFand (f) DOX-MNPs with ACMF.

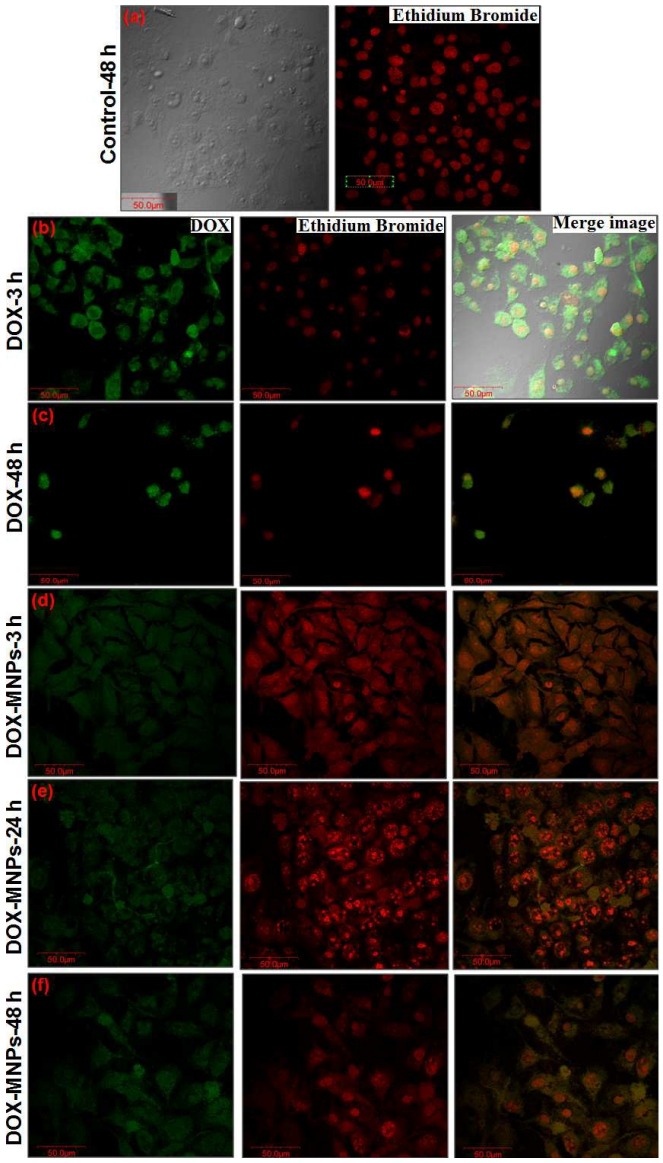

Fig.9. Confocal laser scanning microscopy (CLSM) images show the apoptosis (DNA fragmentation) in (a) Control HeLa cells showing rounded, intact nucleus, (b-c) with DOX (7µg/ml) at indicated time intervals of 3 and 48 h, (d-e) with DOX-MNPs (100µg/ml) at indicated time intervals of 3, 24 and 48 h. The green fluorescence shows the presence of DOX in DOX-MNPs, red fluorescence shows ethidium bromide (EtBr) stained nuclei. The scale bar is 50 µm.